JACS
JOURNAL OF THE AMERICAN CHEMICAL SOCIETY
pubs.acs.org/JACS
Article

Hydrolysis-Resistant Ester-Based Linkers for Development of Activity-Based NIR Bioluminescence Probes

Anuj K Yadav, Zhenxiang Zhao, Yourong Weng, Sarah H Gardner, Catharine J Brady, Oliver D Pichardo Peguero, and Jefferson Chan*

Cite This: J. Am. Chem. Soc. 2023, 145, 1460–1469
Read Online
ACCESS | Metrics & More | Article Recommendations | Supporting Information

ABSTRACT: Activity-based sensing (ABS) probes equipped with a NIR bioluminescence readout are promising chemical tools to study cancer biomarkers owing to their high sensitivity and deep tissue compatibility. Despite the demand, there is a dearth of such probes because NIR substrates (e.g., BL660 (a NIR luciferin analog)) are not equipped with an appropriate attachment site for ABS trigger installation. For instance, our attempts to mask the carboxylic acid moiety with standard self-immolative benzyl linkers resulted in significant background signals owing to undesirable ester hydrolysis. In this study, we overcame this longstanding challenge by rationally designing a new hydrolysis-resistant ester-based linker featuring an isopropyl shielding arm. Compared to the parent, the new design is 140.5-fold and 67.8-fold more resistant toward spontaneous and esterase-mediated hydrolysis, respectively. Likewise, we observed minimal cleavage of the ester moiety when incubated with a panel of enzymes possessing ester-hydrolyzing activity. These impressive in vitro results were corroborated through a series of key experiments in live cells. Further, we showcased the utility of this technology by developing the first NIR bioluminescent probe for nitroreductase (NTR) activity and applied it to visualize elevated NTR expression in oxygen deficient lung cancer cells and in a murine model of non-small cell lung cancer. The ability to monitor the activity of this key biomarker in a deep tissue context is critical because it is associated with tumor hypoxia, which in turn is linked to drug resistance and aggressive cancer phenotypes.

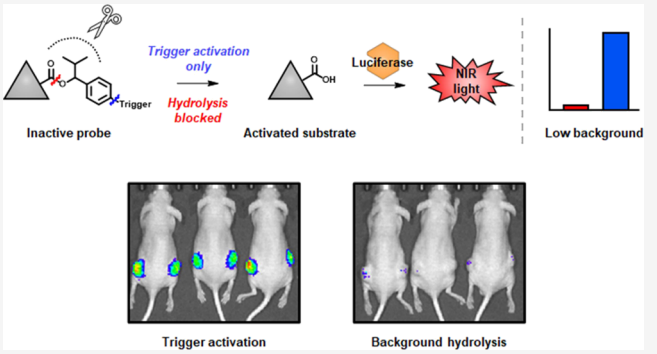

INTRODUCTION

The bioavailability and cell permeability of small-molecule drugs, imaging agents, or activity-based sensing (ABS) probes are largely dictated by molecular weight, lipophilicity, hydrogen bonding ability and net charge.[1,2] For instance, a positively charged or neutral molecule is more likely to gain entry into a cell compared to an anion owing to Coulombic repulsion caused by the negatively charged membrane. A reliable strategy to improve cell uptake is to temporarily mask the negative functional group. For example, carboxylates can be readily transformed into the corresponding ester moiety, which upon crossing the cell membrane, can be cleaved to unmask the latent charge via intracellular esterase activity.[3,4] A notable example is the use of this strategy to facilitate uptake of fluorescent indicators for calcium, which are equipped with a tri- or tetra-carboxylate binding motif.[5,6] Under normal circumstances, it would be nearly impossible for a molecule with a net charge of −3 or −4 to enter the cell. However, calcium indicators for cellular imaging are routinely prepared and sold in the acetoxy methyl ester form. Beyond the modification of small molecules, this approach has extended to facilitate the delivery of functional proteins through the conversion of surface-exposed carboxylates to esters. Elegant examples include the delivery of GFP[7] and human ribonuclease 1.[8] However, there are limitations that must be considered when carboxylate-masking is employed in vivo for the purpose of targeted cargo delivery. First, most esters are prone to spontaneous hydrolysis under acidic, neutral, or basic conditions.[9,10] The body features numerous pH gradients (e.g., the pH in the gastrointestinal tract ranges from 5.7 to 7.4), which will result in off-target delivery upon systemic administration. Second, ester-hydrolyzing enzymes are ubiquitously expressed throughout the body in nearly all cell types, leading to indiscriminate cargo release. In general, ester stability is correlated to size and this property has been leveraged to tune the pharmacokinetics of drugs such as androgens. For instance, the in vivo half-life of testosterone

Received: December 6, 2022
Published: January 5, 2023

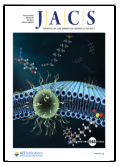

https://doi.org/10.1021/jacs.2c12984
J. Am. Chem. Soc. 2023, 145, 1460–1469

esters can be increased from the 2−3-day range (propionate ester) to over 12 weeks (undeconate ester) by simply varying the length of the alkyl chain.[11] In the context of ABS,[12−14] an assortment of ester-based probes exists; however, an important distinction is that the carboxylate is a component of the trigger and not of the reporter.[15−26]

Amongst the ABS probes designed for in vivo applications,[27,28] those equipped with a bioluminescence (BL) readout are highly coveted. Unlike fluorescence-based probes which require external light excitation to generate a signal, BL results from luciferase-mediated light production and thus, is highly sensitive due to low background.[29,30] Moreover, the structure of luciferase substrates can be modified to shift the emission wavelength into the NIR,[31−33] as we have done recently, to achieve greater tissue penetration.[34] Regardless of the variant, a viable substrate must contain a free carboxylate group for enzyme recognition and subsequent light generation.[35,36] Unfortunately, the presence of a negative charge adversely impacts cell permeability. To yield an appreciable BL signal in vivo, luciferin must be administered systemically at exorbitant levels (>150 mg/kg). Recently, we reported the development of BL660-NO (a nitric oxide (NO)-responsive probe) by amidating the carboxylate of BL660 (a NIR BL substrate) with *O*-phenylene diamine.[34] We found that this modification dramatically improved cell permeability (in vivo dosing decreased to 1 mg/kg), prompting us to explore the installation of other triggers at this position. However, upon surveying the literature, we discovered the available options were limited to hydrolytically stable groups (e.g., amides,[37] aldehydes,[38] etc.), with a few examples of simple esters.[39,40] We hypothesize the apparent void in this research space is likely due to the general instability of esters in vivo (Scheme 1).

Scheme 1. (a) Schematic Demonstrating the Use of Standard Self-Immolative Linkers to Install ABS Triggers Will Lead to High Background; (b) Linkers Based on Hydrolysis-Resistant Ester Ameliorates This Concern

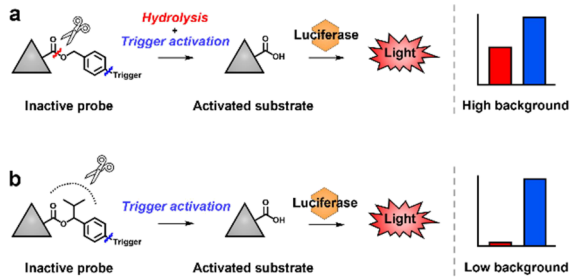

In this study, we report the successful development of a new hydrolysis-resistant ester. Moreover, we show that carboxylate-masking using this ester is generalizable through the modification of two sets of molecules, BL660 and methotrexate (a potent anticancer and immunosuppressive drug). Importantly, we converted the optimized ester to a new self-immolative linker, which we used to develop an ester-based probe to sense nitroreductase (NTR) activity in tumors. The utility of the resulting probe (BL660-NTR) was showcased in A549 lung cancer cells, as well as in a murine model of lung cancer via NIR BL imaging.

RESULTS AND DISCUSSION

Design and Synthesis of Substituted Benzyl Esters. Because the primary objective of this work is to develop ABS probes for the BL modality via carboxylate-masking, we chose to investigate the potential of benzyl esters. Triggers based on *para*-substituted benzyl alcohol, are the most ubiquitous self-immolative linkers used in modern probe design.[41,42] Typically, an electron-deficient analyte-responsive trigger occupies the *para*-position, and the immolative linker is connected to a reporter through a stable ether, carbamate, or carbonate bond. Upon interaction with the target analyte, the trigger is activated to yield a more electron-rich moiety. Flow of electron density into the aromatic ring facilitates formation of a quinone methide (or aza-quinone methide) intermediate which is coupled to the spontaneous release of the latent reporter. We hypothesized inclusion of additional phenyl or alkyl groups at the benzyl position can impart stability by shielding the ester from water or other nucleophiles.[43] Further, we envisioned installing these onto BL660 would enable monitoring of stability using BL imaging. Our envisioned panel of esters initially consisted of **1** (Ph,H), **2** (Ph_2), **3** (PhMe), and later, included optimized ester **4** (Ph,^{i}Pr) shown in Figure 1a.

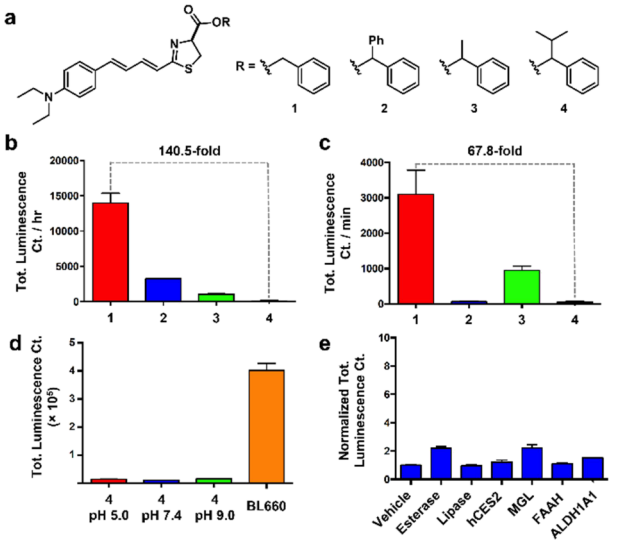

Figure 1. (a) Chemical structures of BL660 esters 1−4. (b) Total luminescence count per hour for compounds 1, 2, 3, and 4 (10 μM) incubated in PBS (pH 7.4) at 37 °C for 1, 6, and 12 h. (n = 3) (c) Total luminescence count per minute for compounds 1, 2, 3, and 4 (10 μM) after treatment with porcine liver esterase (0.1 units/mL) at 37 °C for 20, 40, and 60 min. (n = 3) (d). Total luminescence count for compound 4 (10 μM) at pH 5.0, 7.4, and 9.0 at 37 °C after 2 h incubation. BL600 at the same substrate concentration was added for comparison (n = 3). (e) Normalized total luminescence count for compound 4 (5 μM) exposed to various ester-hydrolyzing enzymes. (n = 3). Total volume of the reaction mixture was maintained at 100 μL with 0.5% DMSO. Final concentration of ATP-Mg and $MgSO_4$ was 4 and 8 mM, respectively. Luciferase = 0.0125 mg/mL.

While the synthesis of **1**−**3** was routine, the esterification of BL660 to afford **4** proved to be challenging owing to the bulky nature of this benzyl alcohol. Conventional reaction conditions to form esters including Fischer, Mitsunobu, Steglich and Yamaguchi esterification failed to give products in appreciable yields beyond trace conversion. Moreover, we observed

https://doi.org/10.1021/jacs.2c12984
J. Am. Chem. Soc. 2023, 145, 1460−1469

racemization of the chiral center housing the carboxylate. This is detrimental because stereochemistry at this position is required for luciferase recognition. Similarly, activation to the acyl chloride, followed by addition of the benzyl alcohol gave complex, inseparable mixtures. Our efforts to control the rate of alcohol addition, molarity of the reaction, stoichiometry of the components, and temperature were all unsuccessful. We also found that diazo chemistry was incompatible with our system.[44] Ultimately, we employed cyanuric fluoride at −20 °C to access the less reactive acyl fluoride intermediate,[45] which upon reaction with the corresponding benzyl alcohol yields the desired ester. Of note, no attempts were made to separate the stereoisomers for **3** and **4**. All subsequent analyses were performed on the mixtures and reported as 'apparent' results.

Assessment of Hydrolytic Stability and Esterase Reactivity. We began our analysis of stability by incubating BL660 esters **1**−**3** at 37 °C in PBS (pH 7.4). After 1, 6, and 12 h, luciferase was added to initiate BL production. The rate of hydrolysis, reported as total luminescence counts per hour, indicates hydrolysis in descending order is: **1** ($13.9 \pm 1.4 \times 10^3$), **2** ($3.3 \pm 0.6 \times 10^3$), and **3** ($1.0 \pm 0.1 \times 10^3$) (Figures 1b and S1). These results show the methyl substituent is over three-fold more effective at blocking hydrolysis than the phenyl group. We speculate hydrolysis of **3** may involve an S_N1 mechanism, thus favoring formation of a double benzylic carbocation. On the contrary, when the panel was treated with porcine liver esterase (0.1 units/mL, 37 °C, pH 7.4) for 20, 40, and 60 min, we found that **2** was most resistant toward enzymatic degradation. It is noteworthy that we selected this source of esterase because it is sold as a mixture of multiple isozymes and thus, will give us the maximum enzyme coverage.[46] The enzymatic rates, reported as total luminescence counts per minute, in descending order are: **1** ($31.0 \pm 6.8 \times 10^2$), **3** ($9.5 \pm 1.2 \times 10^2$), and **2** ($0.6 \pm 0.1 \times 10^2$) (Figures 1c and S2). The greater stability imparted by the aromatic ring is not surprising since esterase reactivity can be readily attenuated with bulkier substituents. With this data, we hypothesized the hydrolytic stability of **3** can be retained (or improved) by switching to a larger alkyl group with multiple rotatable bonds (i.e., isopropyl (^{i}Pr)), while simultaneously suppressing esterase reactivity. To our delight, we observed significant improvements of both properties with this modification. Relative to the parent benzyl ester, **4** is 140.5-fold more resistant to hydrolysis and exhibits 67.8-fold greater esterase stability (Figure 1b,c).

Following this set of experiments, we subjected **4** to acidic (pH 5) and alkaline (pH 9) conditions to account for the various pH gradients in the body. For these experiments we used the Britton−Robinson buffer system. As reported in total luminescence counts per hour, **4** was most stable at pH 7.4 ($8.6 \pm 1.3 \times 10^2$), followed by pH 5.0 ($25.7 \pm 9.6 \times 10^2$), and finally pH 9.0 ($52.8 \pm 20.7 \times 10^2$) (Figure S3). When the BL signal observed after **4** was incubated for 2 h at pH 5.0, 7.4, and 9.0 is compared to the intensity of BL660 at same substrate concentration (5 μM), it is evident that the extent of hydrolysis is negligible (Figures 1d and S4). Lastly, we examined the stability of **4** against a panel of enzymes beyond porcine liver esterase that are known to possess ester-cleaving activity. These include lipase, human carboxyesterase-2, monoacylglycerol lipase, fatty acid amide hydrolase, and aldehyde dehydrogenase 1A1. Remarkably, exposure to high levels of these enzymes over a period of 1 h resulted in minimal activation (Figure 1e). Moreover, compared to BL660 at the same substrate concentration, enzyme-mediated hydrolysis was minimal (Figure S5).

Demonstration of Ph^{i}Pr Ester Stability in Live Cells. Next, we designed a series of two complementary cellular experiments to determine whether the excellent in vitro performance noted above translates within a more complex cellular environment where many esterase isoforms are present.[47] Moreover, we aimed to determine whether the Ph^{i}Pr ester will have a similar effect on other molecules with diverse chemical structures beyond BL660.

First, we prepared BL660-Me, a methyl ester derivative of BL660 (Figure 2a). Next, we cultured 4T1 murine breast

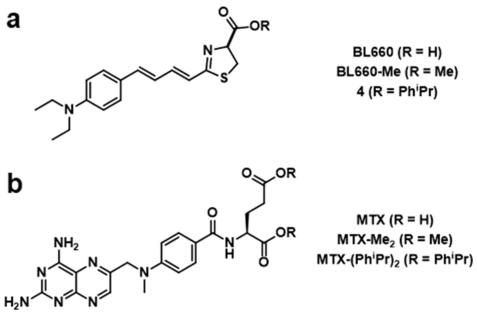

Figure 2. Chemical structures of (a) BL660 and (b) MTX and the Me and Ph^{i}Pr ester derivatives.

cancer cells, stably expressing the luciferase enzyme (4T1-Luc). Of note, we previously showed that BL660 and related substrates are non-toxic in this cell line.[34] The cells were then treated with a DMSO vehicle control, BL660-Me or compound **4** (Figures 3a and S6). We postulate that the BL signal will be

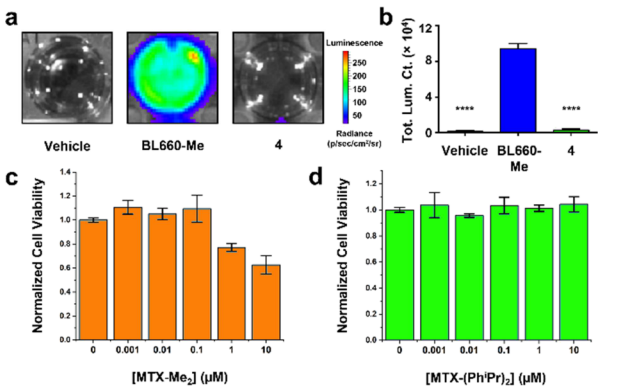

Figure 3. Representative BL images of 4T1-Luc cells plated in 24-well plates treated with (a) DMSO (vehicle); BL660-Me; or Compound 4 for 30 min at 37 °C. Probe concentration = 10 μM. (b) Quantified data from (a). n = 4. MTT viability assays of A549 cells treated with (c) MTX-Me$_2$ or (d) MTX-(Ph^{i}Pr)$_2$ at various concentrations for 24 h. n = 3. Error bars = SEM. Exposure time, 60 s; emission, open; binning factor, 8; and f number, 1. Statistical analysis was performed using a two-tailed t-test (α = 0.05, **** $P < 0.001$).

lower if the optimized ester is indeed more stable in live cells since less of the luciferase substrate will be liberated and made available to generate light. Analysis of the imaging results revealed that the total luminescence count for BL660-Me-treated 4T1 cells ($94.1 \pm 5.9 \times 10^3$) were 55-fold and 31-fold more luminescent relative to the vehicle ($1.7 \pm 0.8 \times 10^3$) and compound **4** ($3.1 \pm 1.2 \times 10^3$) counterparts, respectively

https://doi.org/10.1021/jacs.2c12984
J. Am. Chem. Soc. 2023, 145, 1460−1469

Scheme 2. Schematic Showing NTR-Mediated Activation of BL660-NTR to Afford BL660[a]

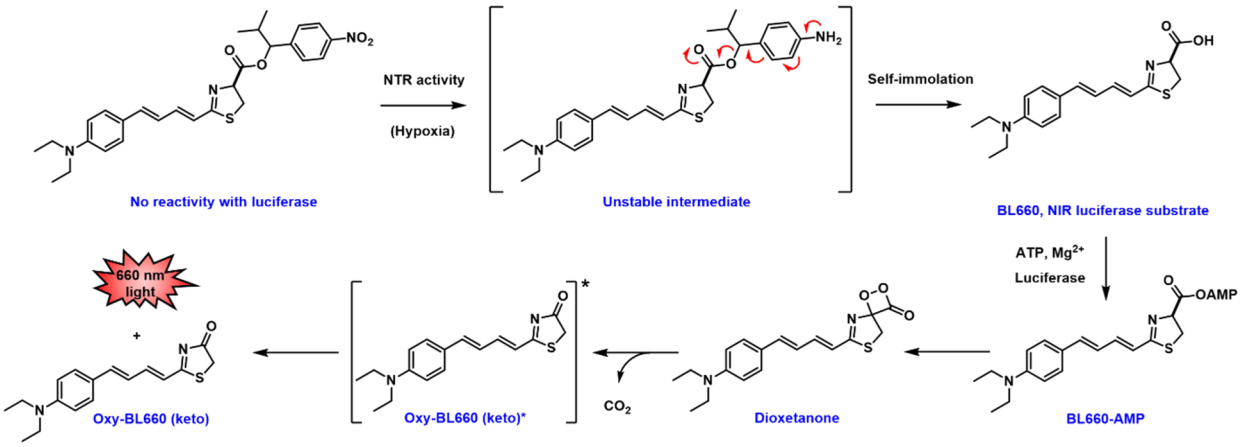

[a]Subsequent luciferase-catalyzed conversion to the dioxetanone intermediate is followed by spontaneous decomposition to the oxy-BL660 in the keto form to generate NIR BL.

(Figure 3b). These results indicate the Ph^{i}Pr ester is stable to the collection of intracellular esterases present in 4T1 cells.

Next, we modified the two carboxylates in methotrexate (a potent anticancer and immunosuppressive drug)[48] to afford the methyl (MTX-Me$_2$) or Ph^{i}Pr (MTX-(Ph^{i}Pr)$_2$) ester variants (Figure 2b). Structure−activity relationship analysis has shown that carboxylate masking decreases target engagement, leading to a significant reduction of cytotoxicity. We hypothesized if the Ph^{i}Pr esters installed onto methotrexate remain intact, cells treated with MTX-(Ph^{i}Pr)$_2$ will remain viable. For this study, we employed A549-Luc2 cells to include analysis in human cancer cells. Cells were treated with MTX-Me$_2$ or MTX-(Ph^{i}Pr)$_2$ at various concentrations for 24 h before they were subjected to MTT analyses. Our results revealed the viability was ∼63 and 100% at the highest concentration (10 μM) of MTX-Me$_2$ and MTX-(Ph^{i}Pr)$_2$ tested, respectively (Figure 3c,d). In comparison, the IC$_{50}$ value of MTX is ∼35 nM in A549 cells.[49] Overall, this experiment demonstrates that the hydrolysis of the esters on MTX-(Ph^{i}Pr)$_2$ is sufficiently slow that the buildup of MTX was inconsequential to the health of the cells.

Conversion of Ph^{i}Pr Ester into a Versatile Self-Immolative Linker. While we envision nearly any electron-deficient trigger can be installed at the *para* (or *ortho*) position of the Ph^{i}Pr ester to yield an ABS probe for NIR BL imaging, we strategically selected to use the nitro group to develop BL660-NTR. In addition to its common use in probe design for other modalities,[50] this biomarker is a feature of gram positive and negative bacteria and thus, can be leveraged for sensing bacterial infections.[51] Moreover, NTR can also be employed to detect tumor hypoxia owing to overexpression in many types of solid tumors.[52] Once our probe engages its target, the aryl nitro moiety can be reduced to afford the electron-rich hydroxylamine or amino products, which initiates self-immolation to release BL660. In the presence of luciferase, this substrate is then enzymatically converted to a dioxetanone, which decomposes to generate oxy-BL660 in an excited state. Relaxation to the ground state is accompanied by the emission of a photon at 660 nm (Scheme 2).

The synthesis of BL660-NTR began with subjecting 4-nitro iodobenzene to phenyllithium to initiate a lithium-halogen exchange reaction. The resulting 4-nitrophenyllihtium intermediate was used directly without purification to attack 2-methyl propanaldehyde to give benzyl alcohol **5** in 25% yield. Then utilizing the acyl fluoride chemistry we optimized above, BL660-NTR was obtained in 10% yield (Figure 4a).

With BL660-NTR in hand, we designed a fluorescent (FL)-based experiment to compare its hydrolytic stability to that of the primary alcohol ester analog (Supporting Information Scheme 3). Of note, the use of FL, rather than BL, allowed us to quantify the percent of probe hydrolyzed by construction of a calibration curve using BL660 (Figure S7). When intact, both compounds are weakly fluorescent; however, hydrolysis leads to separation of BL660 from the linker containing the aryl nitro trigger (which acts as a quencher). This results in a fluorescence signal increase which we use to determine the extent of cleavage. After an incubation of 24 h in PBS at 37 °C, only 1.6 ± 0.1% of BL660-NTR was hydrolyzed; however, 28.3 ± 0.1% of the primary alcohol ester was cleaved under the same conditions (Figures 4b,c, and S8). We observed an even more dramatic difference when the two probes were treated with porcine liver esterase for 1 h. In this experiment, 1.9 ± 0.2% of BL660-NTR was hydrolyzed, whereas the majority of the primary alcohol ester (78.7 ± 0.2%) was consumed (Figure S9). Next, we performed an in vitro assay to demonstrate that the BL output depends on both NTR and luciferase activity (Figures 4d and S10). When each component is present, we observed a notable increase in the total luminescence count. However, when NTR (column 2) was absent, the signal was significantly attenuated. Likewise, when luciferase (column 3) or BL660-NTR (column 4) was excluded from the reaction, the signal was minimal and comparable to control wells containing only media and a DMSO vehicle. Next, we subjected BL660-NTR to various biologically relevant analytes that may contribute to off-target probe activation in vivo. For instance, transition metals like Cu(II) can facilitate ester hydrolysis via Lewis acid-mediated ester activation.[53] Additionally, various reactive oxygen and nitrogen that can interact with the ester bond were also tested. Lastly, we also examined reactive sulfur species, which are known to reduce aryl nitro groups.[47] Under no circumstance did we observe activation greater than 10% compared to the NTR positive control (Figure 4e). Additional assays such as dose dependent NTR studies (Figure S11) can be found in the Supporting Information document.

https://doi.org/10.1021/jacs.2c12984
J. Am. Chem. Soc. 2023, 145, 1460−1469

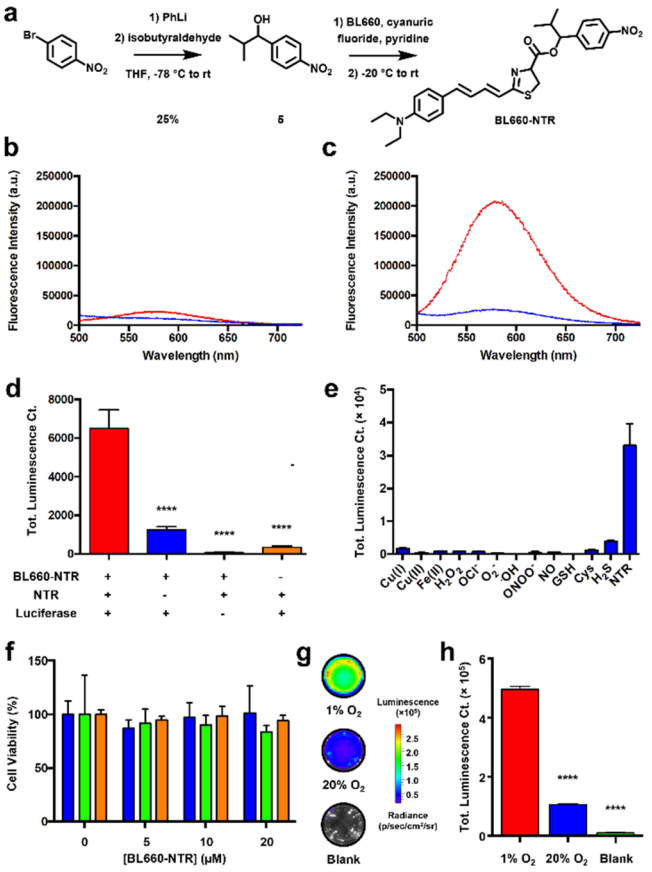

Figure 4. (a) Synthetic route to access BL660-NTR. FL emission spectra of (b) BL660-NTR and the (c) primary alcohol ester analog before (blue) and after (red) incubation in PBS (pH 7.4) at 37 °C for 24 h. (d) In vitro assay demonstrating that the probe, NTR, and luciferase must all be present to generate a signal: BL660-NTR (5 μM), NTR (0.1 units), and luciferase (0.0125 mg/mL final concentration). (e) Response to biologically relevant analytes that may cause interference. (f) MTT assay at various concentrations of BL660-NTR (0, 5, 10, 20 μM). Blue, green, and orange represents 1-, 3-, and 24-h incubation, respectively. (g) Representative BL images of A549 cell lysates obtained after cells were cultured in a 1 or 20% oxygen atmosphere for 2 days prior to incubation with BL660-NTR for 60 min, (h) Quantified data from (g). n = 4. Error bars = SEM. Exposure time, 60 s; emission, open; binning factor, 8; and f number, 1. Statistical analysis was performed using a two-tailed t-test (α = 0.05, **** P < 0.001).

Prior to testing BL660-NTR in vivo, we assessed potential cytotoxicity by treating A549 cells with BL660-NTR across a concentration range of 0 to 20 μM for up to 24 h. No loss of cell viability was observed (Figure 4f). Next, we performed a cell imaging study to measure NTR activity within a living system. Specifically, A549 cells (not expressing Luc) were cultured in an atmosphere consisting of 1 or 20% oxygen for 2 days. Because aryl nitro reduction mediated by mammalian NTRs can be inhibited by molecular oxygen, we expect there to be greater probe activation under oxygen-deficient conditions.[54] After incubating with BL660-NTR for 60 min, the cells were washed with fresh PBS, detached, pelleted, and lysed via sonication. The lysates were then transferred to 24-well plates, treated with luciferase and imaged immediately using the IVIS imaging system. Of note, the concentration of NTR in lysates from this cell line is 13.6 μg/mL.[55] As shown in Figure 4g, wells containing lysates obtained from the cells incubated under hypoxic conditions (5.0 ± 0.1 × 10^5 total luminescent counts) were significantly brighter than the corresponding normoxic lysates (1.1 ± 0.03 × 10^5 total luminescent counts) (Figures 4h and S12). This represents a significant 4.5-fold difference in BL intensity.

In Vivo Application of BL660-NTR to Detect Tumor NTR Activity. Finally, we employed BL660-NTR in vivo to image NTR activity in tumors. Owing to the established inhibitory effect of oxygen on NTR-mediated aryl nitro reduction (Figure S13), NTR activity is often used as a proxy for hypoxia in the preclinical and clinical arenas.[56,57] Hypoxia is defined as a condition where the demand for oxygen from rapidly dividing cancer cells, outweigh the available supply. This condition emerges as the distance between the cancer cells and nutrient-rich blood vessels become greater as a function of tumor growth.[58] Of note, although several NTR probes for BL have been developed previously,[52,59−62] BL660-NTR is the first example capable of deep-tissue detection of NTR activity via NIR BL imaging.

NU/J mice (male, ∼5-weeks old) were inoculated with A549-Luc2 lung cancer cells (5 × 10^6) in both flanks. Testing of BL660-NTR commenced after tumors had grown to a volume of ∼300 mm^3 (∼4 weeks). First, we performed imaging using BL660-NTR, which was administered systemically via retroorbital injection (Figures 5a and S14). ROIs were drawn around each tumor and the luminescent count was summed for each animal. By the first scan (5 min), strong BL signals were apparent in all tumors. The BL intensity appears to decrease slightly after 15 min and levels off until the end of the experiment (75 min) (Figure 5c). After 20 h, the BL signal had completely dissipated, indicating full consumption or

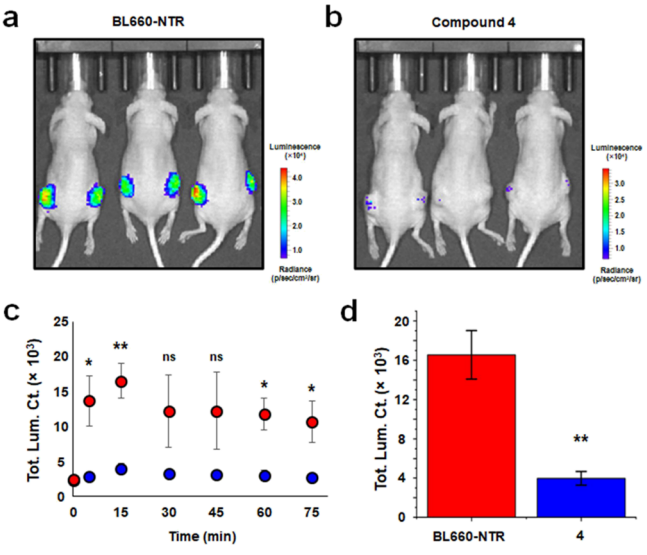

Figure 5. Bioluminescence images of NU/J mice bearing A549-Luc2 tumors acquired 15 min after systemic administration of (a) BL660-NTR or (b) compound 4. Injection volume = ∼100 μL (3:7 v/v DMSO:PBS). Stock concentration of BL660-NTR and 4 = ∼582 μM. (c) Total luminescence count of animals treated with BL660-NTR (red circles) or compound 4 (blue circles). Data acquired at time = 0 min (before injection) and at 5, 15, 30, 45, 60, and 75 min after injection. (d) Quantification of imaging data from 15 min time point. n = 3 for all experiments. Error bars = SEM. Exposure time, 60 s; emission, open; binning factor, 8; and f number, 1. Statistical analysis was performed using a two-tailed t-test (α = 0.05, * P < 0.05, ** P < 0.01, ns = not significant).

https://doi.org/10.1021/jacs.2c12984
J. Am. Chem. Soc. 2023, 145, 1460−1469

complete clearance of the probe. At this point, compound **4** was administered and imaged as before (Figures 5b and S15). Because the only difference between **4** and **BL660-NTR** is that the nitro trigger is absent (Figure 1a), this allows us to distinguish between NTR activation and off-target ester hydrolysis by comparing the BL signal between the two imaging sessions. Despite dosing at the same concentration, the BL signal in the tumors at all time points were barely discernable from background (Figure 5c). The total luminescent count after 15 min for compound **4** was only $4.0 \pm 0.7 \times 10^3$, whereas the corresponding readout was $16.6 \pm 2.5 \times 10^3$ for BL660-NTR. This represents a 5.2-fold difference, indicating successful detection of NTR activity in tumors (Figure 5d).

CONCLUSIONS

The growing diversity of ABS probes for BL imaging has enabled the study of various important analytes using luciferase-expressing cells and animal models.[30,63] Most of these examples are prepared by capping the phenolic alcohol of luciferin (or related molecules)[64−71] with an analyte-responsive trigger,[60,72−84] which upon removal can interact with luciferase to yield BL. While luciferin and probes derived from this parent molecule boast excellent BL properties (e.g., strong signal output), the emission wavelength is still in the visible window (λ_{max} = ∼560 nm),[85] limiting the attainable imaging depth. A transition to the NIR region (>650 nm) can improve tissue penetration since there are less optical absorbers (e.g., amino acids and nucleic acids) that can intercept, and scatter the emitted light. However, red-shifting luciferase substrates often entails exchanging the alcohol group with a dialkylamino substituent, which prevents installation of triggers at this position. This was in fact the case with NIR emitting BL660, which features a *N*,*N*-diethylamino group. Thus, our only option was to cap the carboxylate with a trigger; however, as discussed previously, the variety of suitable triggers are severely limited.

In this work, we overcame this limitation by rationally developing a hydrolysis-resistant ester that is also remarkably stable against enzymatic degradation. By installing a trigger at the *para*- or *ortho*-positions of this ester, we can leverage self-immolative chemistry to afford NIR ABS probes via carboxylate-masking and subsequent unmasking. Specifically, inclusion of a nitro group transformed the Ph^{i}Pr ester into an ABS linker for NTR activity. Our probe, BL660-NTR, is the first NIR BL probe for this target, and only the second NIR emitting ABS probe ever developed. Beyond sensing NTR activity, our new self-immolative linker can be readily adapted to develop probes for other analytes.

In addition to modifying BL660, we have also successfully masked methotrexate, which is notorious for severe side-effects when administered to patients owing to non-specific destruction of healthy cells. Moreover, carboxylates are found in many other medications, including antibacterial agents (ceftazidime, ciprofloxacin, and sulbactam). As such, the pursuit of prodrugs via carboxylate masking using our technology is an exciting avenue.

EXPERIMENTAL DETAILS

2-Methyl-1-(4-nitrophenyl)propan-1-ol (5). A solution of phenyllithium in dibutyl ether (1.9 M, 1.69 mL, 3.21 mmol, 1 equiv) was slowly added to a cooled (−78 °C) solution of 4-nitro iodobenzene (0.8 g, 3.21 mmol, 1 equiv) in anhydrous THF (16 mL) under N_2. The reaction was stirred for 45 min at the same temperature to afford the 4-nitrophenyllihtium intermediate in situ, then a solution of isobutyraldehyde (0.32 mL, 3.50 mmol, 1.1 equiv) in anhydrous THF (3 mL) was added dropwise. The reaction was stirred for an additional 1 h at −78 °C before warming to room temp. The reaction mixture was then quenched with saturated aqueous NH_4Cl, transferred to a separatory funnel, and extracted with diethyl ether (3×). The combined organic layers were dried over Na_2SO_4, filtered, concentrated, and purified using silica gel column chromatography (eluent: 3:17 v/v EtOAc:Hexanes) to afford **5** in 20% yield. (0.126 g, 0.64 mmol). ^{1}H NMR (500 MHz, $CDCl_3$) δ 8.20 (d, J = 8.9 Hz, 2H), 7.49 (d, J = 8.7 Hz, 2H), 4.56 (dd, J = 6.1, 3.2 Hz, 1H), 2.01−1.94 (m, 2H), 0.95 (d, J = 6.7 Hz, 3H), 0.87 (d, J = 6.9 Hz, 3H). ^{13}C NMR (126 MHz, $CDCl_3$) δ 17.50, 19.01, 35.56, 78.81, 123.53, 127.41, 147.38, 151.05. HRMS $[M + H]^+$ calculated mass for $C_{10}H_{14}NO_3$ = 196.09737, found = 196.09733.

BL660-NTR. A solution of BL660 (17.3 mg, 0.052 mmol, 1 equiv) and pyridine (4.23 mL, 0.052 mmol, 1 equiv) in anhydrous CH_2Cl_2 (1.5 mL) was cooled to −20 °C under the N_2 atmosphere. Cyanuric fluoride (4.85 mL, 0.056 mmol, 1.08 equiv) was slowly added to the reaction and stirred at the same temp. For ∼40 min. A solution of compound **5** (28.6 mg, 0.146 mmol, 2.8 equiv) in anhydrous CH_2Cl_2 (0.5 mL) was added dropwise at the same temperature. The reaction was slowly brought to room temperature and was stirred for an additional 1.5 h at room temperature. After quenching with crushed ice, the organic layer was removed, and the aqueous layer was extracted with CH_2Cl_2. The combined organic layers were dried over Na_2SO_4, filtered, concentrated, and purified using silica gel column chromatography (eluent: 1:4 v/v EtOAc:Hexanes) to afford BL660-NTR in 10% yield (2.7 mg, 0.005 mmol). ^{1}H NMR (400 MHz, $CDCl_3$) δ 8.25−8.16 (m, 2H), 7.48 (d, J = 8.7 Hz, 2H), 7.33 (d, J = 8.5 Hz, 2H), 7.00−6.90 (m, 1H), 6.80−6.57 (m, 4H), 6.56−6.48 (m, 1H), 5.61 (d, J = 6.7 Hz, 1H), 5.27−5.19 (m, 1H), 3.53 (t, J = 8.3 Hz, 2H), 3.44−3.33 (m, 4H), 2.24−2.11 (m, 1H), 1.18 (t, J = 7.1 Hz, 6H), 1.00 (d, J = 6.7 Hz, 3H), 0.85 (d, J = 3.5 Hz, 3H). ^{13}C NMR (150 MHz, CD_2Cl_2) δ 12.76, 14.28, 18.07, 18.23, 18.70, 18.77, 23.10, 29.76, 30.09, 32.33, 34.06, 34.09, 35.06, 44.79, 64.45, 69.55, 78.35, 81.07, 81.12, 111.77, 122.29, 123.82, 123.87, 128.08, 128.16, 128.76, 129.14, 129.86, 131.29, 133.33, 140.07, 147.20, 170.41. HRMS $[M + H]^+$ calculated mass for $C_{28}H_{34}N_3O_4S$ = 508.2270, found = 508.2262.

MTT Assay Using MTX-Me$_2$ and MTX-Ph^{i}Pr$_2$. 48-well plates were seeded with 30,000 A549 cells per well (500 μL of 60,000 cells/mL) and incubated at 37 °C with 5% CO_2 for 24 h. Media was removed and fresh serum-free RPMI 1640 containing 0, 0.001, 0.01, 0.1, 1, 10 μL of MTX-Me$_2$ or MTX-(Pr^{i}Pr)$_2$ were added (0.1% DMSO final v/v). The media was removed after 24 h incubation and replaced with 500 μL of a 20:1 mixture of serum-free RPMI 1640 and (3-(4,5- dimethylthiazol2-yl)-2,5-diphenyl-tetrazolium bromide (MTT, 5 mg/mL stock in PBS). The cells were incubated for 2 h under the same condition and then the medium was removed and replaced with DMSO (500 μL/well). The absorbance of each well was recorded at 555 nm on a microplate reader. Viability was calculated by the absorbance relative to the vehicle control.

Detection of NTR Activity in A549 Lung Cancer Cells. A549 cells were seeded in T75 culture flasks and incubated in 1 or 20% oxygen atmosphere for 48 h. A solution of BL660-NTR in DMSO (2 mM, 50 μL) was quickly added into each flask such that the final concentration of the probe is 10 μM and 0.5% DMSO. The cells were incubated with the probe for 60 min (under the respective culture conditions), washed with fresh PBS, and detached from the culture flasks. The cells were then transferred to a 15 mL centrifuge tube and pelleted at 1000 rpm for 5 min at room temp. The cells (4.25×10^6 cells/mL) were then resuspended in PBS along with 10% protease inhibitor solution (1 protease inhibitor mini tablet per 10 mL PBS, Pierce, Thermo Fisher Scientific) and sonicated on ice for 2.5 min (pulse 01, 01, 40%). The cell debris was removed via centrifugation at 4 °C. The cell lysates were further diluted 2.5-fold by PBS and 475 μL were transferred into 24-well plates (n = 4 for each condition), treated with luciferase (25 μL, 0.25 mg/mL), and imaged immediately using the IVIS imaging system. Bioluminescence light was collected in open

https://doi.org/10.1021/jacs.2c12984
J. Am. Chem. Soc. 2023, 145, 1460−1469

mode (no filters were applied). ROIs were drawn around each well. The signal intensity was quantified using the Living Image Analysis Software.

BL Imaging of NTR Activity in a Lung Cancer Model. NU/J mice bearing A549-Luc2 tumors were anesthetized using isoflurane (1−3% for maintenance; up to 5% for induction) in oxygen from a precision vaporizer. After testing to ensure animals are fully under anesthesia, an initial background scan is recorded. BL660-NTR or compound **4** formulated in 3:7 v/v DMSO:PBS (see Supporting Information for details) was then administered via retroorbital injection. Images were captured using the IVIS imaging system at 5, 15, 30, 45, 60, and 75 min after injection. Bioluminescence light was collected in open mode (no filters were applied). ROIs were drawn around each tumor and summed for each animal. The signal intensity was quantified using the Living Image Analysis Software.

■ ASSOCIATED CONTENT

Supporting Information

The Supporting Information is available free of charge at https://pubs.acs.org/doi/10.1021/jacs.2c12984.

Further experimental details, including synthetic procedures, spectral data, and supplemental in vitro and in vivo procedures and data are supplied in the Supporting Information document (PDF)

■ AUTHOR INFORMATION

Corresponding Author

Jefferson Chan − *Department of Chemistry, Beckman Institute for Advanced Science and Technology, and Cancer Center at Illinois and Department of Biochemistry, University of Illinois at Urbana−Champaign, Urbana, Illinois 61801, United States;* orcid.org/0000-0003-4139-4379; Email: jeffchan@illinois.edu

Authors

Anuj K Yadav − *Department of Chemistry, Beckman Institute for Advanced Science and Technology, and Cancer Center at Illinois, University of Illinois at Urbana−Champaign, Urbana, Illinois 61801, United States*

Zhenxiang Zhao − *Department of Chemistry, Beckman Institute for Advanced Science and Technology, and Cancer Center at Illinois, University of Illinois at Urbana−Champaign, Urbana, Illinois 61801, United States*

Yourong Weng − *Department of Chemistry, Beckman Institute for Advanced Science and Technology, and Cancer Center at Illinois, University of Illinois at Urbana−Champaign, Urbana, Illinois 61801, United States*

Sarah H Gardner − *Department of Biochemistry, University of Illinois at Urbana−Champaign, Urbana, Illinois 61801, United States*

Catharine J Brady − *Department of Chemistry, Beckman Institute for Advanced Science and Technology, and Cancer Center at Illinois, University of Illinois at Urbana−Champaign, Urbana, Illinois 61801, United States*

Oliver D Pichardo Peguero − *Department of Chemistry, Beckman Institute for Advanced Science and Technology, and Cancer Center at Illinois, University of Illinois at Urbana−Champaign, Urbana, Illinois 61801, United States*

Complete contact information is available at: https://pubs.acs.org/10.1021/jacs.2c12984

Author Contributions

The manuscript was written through contributions of all authors. All authors have given approval to the final version of the manuscript.

Funding

This work was supported by the National Institutes of Health (R35GM133581) and in part by a grant awarded to J.C. from the Chemistry Discovery Fund established by Ving & May Lee.

Notes

The authors declare no competing financial interest.

■ ACKNOWLEDGMENTS

C.J.B. acknowledges the Chemistry-Biology Interface Training Grant (T32-GM136629) and previous support from the Robert C. and Carolyn J. Springborn Graduate Fellowship. SHG thanks the Cancer Center at Illinois for a Graduate Student Cancer Scholarship. J.C. thanks the Helen Corley Petit Scholar Program and the Camille and Henry Dreyfus Foundation. Major funding for the 500 MHz Bruker CryoProbe was provided by the Roy J. Carver Charitable Trust (Muscatine, Iowa; Grant No. 15-4521) to the School of Chemical Sciences NMR Lab. The Q-Tof Ultima mass spectrometer was purchased in part with a grant from the National Science Foundation, Division of Biological Infrastructure (DBI-0100085). We also acknowledge Dr. Iwona Dobrucka and the Molecular Imaging Laboratory at the Beckman Institute for use of the IVIS imaging system.

■ ABBREVIATIONS

BAPTA	1,2-bis(o-aminophenoxy)ethane-*N*,*N*,*N*′,*N*′-tetraacetic acid
GFP	green fluorescent protein
IC_{50}	half maximal inhibitory concentration
MS	mass spectrometry
MTT	3-(4,5-dimethylthiazol-2-yl)-2,5-diphenyltetrazolium bromide
NIR	near-infrared
NMR	nuclear magnetic resonance
PBS	phosphate-buffered saline
ROI	region of interest
rpm	rotations per minute
SEM	standard error of the mean
S_N1	unimolecular nucleophilic substitution

■ REFERENCES

(1) Lipinski, C. A.; Lombardo, F.; Dominy, B. W.; Feeney, P. J. Experimental and Computational Approaches to Estimate Solubility and Permeability in Drug Discovery and Development Settings. *Adv. Drug Deliv. Rev.* **2001**, *46*, 3−26.

(2) Yang, N. J.; Hinner, M. J. *Getting Across the Cell Membrane: An Overview for Small Molecules, Peptides, and Proteins BT - Site-Specific Protein Labeling: Methods and Protocols*; Gautier, A., Hinner, M. J., Eds.; Springer New York: New York, NY, 2015; 29−53.

(3) Beaumont, K.; Webster, R.; Gardner, I.; Dack, K. Design of Ester Prodrugs to Enhance Oral Absorption of Poorly Permeable Compounds: Challenges to the Discovery Scientist. *Curr. Drug Metab.* **2003**, *4*, 461−485.

(4) Lavis, L. D. Ester Bonds in Prodrugs. *ACS Chem. Biol.* **2008**, *3*, 203−206.

(5) Tsien, R. Y. New Calcium Indicators and Buffers with High Selectivity against Magnesium and Protons: Design, Synthesis, and Properties of Prototype Structures. *Biochemistry* **1980**, *19*, 2396−2404.

(6) Minta, A.; Kao, J. P. Y.; Tsien, R. Y. Fluorescent Indicators for Cytosolic Calcium Based on Rhodamine and Fluorescein Chromophores. *J. Biol. Chem.* **1989**, *264*, 8171−8178.
(7) Mix, K. A.; Lomax, J. E.; Raines, R. T. Cytosolic Delivery of Proteins by Bioreversible Esterification. *J. Am. Chem. Soc.* **2017**, *139*, 14396−14398.
(8) Ressler, V. T.; Mix, K. A.; Raines, R. T. Esterification Delivers a Functional Enzyme into a Human Cell. *ACS Chem. Biol.* **2019**, *14*, 599−602.
(9) Bender, M. L.; Turnquest, B. W. General Basic Catalysis of Ester Hydrolysis and Its Relationship to Enzymatic Hydrolysis [1]. *J. Am. Chem. Soc.* **1957**, *79*, 1656−1662.
(10) Martin, R. B. Acid-Catalyzed Ester Hydrolysis. *J. Am. Chem. Soc.* **1967**, *89*, 2501−2502.
(11) Forsdahl, G.; Erceg, D.; Geisendorfer, T.; Turkalj, M.; Plavec, D.; Thevis, M.; Tretzel, L.; Gmeiner, G. Detection of Testosterone Esters in Blood. *Drug Test. Anal.* **2015**, *7*, 983−989.
(12) Chan, J.; Dodani, S. C.; Chang, C. J. Reaction-Based Small-Molecule Fluorescent Probes for Chemoselective Bioimaging. *Nat. Chem.* **2012**, *4*, 973−984.
(13) Bruemmer, K. J.; Crossley, S. W. M.; Chang, C. J. Activity-Based Sensing: A Synthetic Methods Approach for Selective Molecular Imaging and Beyond. *Angew. Chem., Int. Ed.* **2020**, *59*, 13734−13762.
(14) Gardner, S. H.; Reinhardt, C. J.; Chan, J. Advances in Activity-Based Sensing Probes for Isoform-Selective Imaging of Enzymatic Activity. *Angew. Chem., Int. Ed.* **2021**, *60*, 5000−5009.
(15) Kierat, R. M.; Krämer, R. A Fluorogenic and Chromogenic Probe That Detects the Esterase Activity of Trace Copper(II). *Bioorg. Med. Chem. Lett.* **2005**, *15*, 4824−4827.
(16) Li, H.; Zhang, P.; Smaga, L. P.; Hoffman, R. A.; Chan, J. Photoacoustic Probes for Ratiometric Imaging of Copper(II). *J. Am. Chem. Soc.* **2015**, *137*, 15628−15631.
(17) Kawai, K.; Ieda, N.; Aizawa, K.; Suzuki, T.; Miyata, N.; Nakagawa, H. A Reductant-Resistant and Metal-Free Fluorescent Probe for Nitroxyl Applicable to Living Cells. *J. Am. Chem. Soc.* **2013**, *135*, 12690−12696.
(18) Pino, N. W.; Davis, J., III; Yu, Z.; Chan, J. NitroxylFluor: A Thiol-Based Fluorescent Probe for Live-Cell Imaging of Nitroxyl. *J. Am. Chem. Soc.* **2017**, *139*, 18476−18479.
(19) Liu, C.; Pan, J.; Li, S.; Zhao, Y.; Wu, L. Y.; Berkman, C. E.; Whorton, A. R.; Xian, M. Capture and Visualization of Hydrogen Sulfide by a Fluorescent Probe. *Angew. Chem., Int. Ed.* **2011**, *50*, 10327−10329.
(20) Liu, C.; Peng, B.; Li, S.; Park, C.-M.; Whorton, A. R.; Xian, M. Reaction Based Fluorescent Probes for Hydrogen Sulfide. *Org. Lett.* **2012**, *14*, 2184−2187.
(21) Chen, W.; Liu, C.; Peng, B.; Zhao, Y.; Pacheco, A.; Xian, M. New Fluorescent Probes for Sulfane Sulfurs and the Application in Bioimaging. *Chem. Sci.* **2013**, *4*, 2892−2896.
(22) Hou, Y.; Yang, X.-F.; Zhong, Y.; Li, Z. Development of Fluorescent Probes for Hydrogen Polysulfides by Using Cinnamate Ester as the Recognition Unit. *Sens. Actuators B Chem.* **2016**, *232*, 531−537.
(23) Liu, C.; Chen, W.; Shi, W.; Peng, B.; Zhao, Y.; Ma, H.; Xian, M. Rational Design and Bioimaging Applications of Highly Selective Fluorescence Probes for Hydrogen Polysulfides. *J. Am. Chem. Soc.* **2014**, *136*, 7257−7260.
(24) Choi, M. G.; Hwang, J.; Eor, S.; Chang, S.-K. Chromogenic and Fluorogenic Signaling of Sulfite by Selective Deprotection of Resorufin Levulinate. *Org. Lett.* **2010**, *12*, 5624−5627.
(25) Hu, S.; Wang, J.; Luo, M.; Wu, Z.; Hou, Y.; Chen, X. A Novel ESIPT Fluorescent Probe Derived from 3-Hydroxyphthalimide for Hydrazine Detection in Aqueous Solution and Living Cells. *Anal. Bioanal. Chem.* **2021**, *413*, 5463−5468.
(26) Kailass, K.; Sadovski, O.; Capello, M.; Kang, Y.; Fleming, J. B.; Hanash, S. M.; Beharry, A. A. Measuring Human Carboxylesterase 2 Activity in Pancreatic Cancer Patient-Derived Xenografts Using a Ratiometric Fluorescent Chemosensor. *Chem. Sci.* **2019**, *10*, 8428−8437.
(27) Knox, H. J.; Chan, J. Acoustogenic Probes: A New Frontier in Photoacoustic Imaging. *Acc. Chem. Res.* **2018**, *51*, 2897−2905.
(28) Yadav, A. K.; Hernandez, S.; Su, S.; Chan, J. Acoustic-Based Chemical Tools for Profiling the Tumor Microenvironment. *Curr. Opin. Chem. Biol.* **2020**, *57*, 114−121.
(29) East, A. K.; Lucero, M. Y.; Chan, J. New Directions of Activity-Based Sensing for *in Vivo* NIR Imaging. *Chem. Sci.* **2021**, *12*, 3393−3405.
(30) Su, T. A.; Bruemmer, K. J.; Chang, C. J. Caged Luciferins for Bioluminescent Activity-Based Sensing. *Curr. Opin. Biotechnol.* **2019**, *60*, 198−204.
(31) Evans, M. S.; Chaurette, J. P.; Adams, S. T.; Reddy, G. R.; Paley, M. A.; Aronin, N.; Prescher, J. A.; Miller, S. C. A Synthetic Luciferin Improves Bioluminescence Imaging in Live Mice. *Nat. Methods* **2014**, *11*, 393−395.
(32) Kuchimaru, T.; Iwano, S.; Kiyama, M.; Mitsumata, S.; Kadonosono, T.; Niwa, H.; Maki, S.; Kizaka-Kondoh, S. A Luciferin Analogue Generating Near-Infrared Bioluminescence Achieves Highly Sensitive Deep-Tissue Imaging. *Nat. Commun.* **2016**, *7*, 11856.
(33) Hall, M. P.; Woodroofe, C. C.; Wood, M. G.; Que, I.; van't Root, M.; Ridwan, Y.; Shi, C.; Kirkland, T. A.; Encell, L. P.; Wood, K. V.; Löwik, C.; Mezzanotte, L. Click Beetle Luciferase Mutant and near Infrared Naphthyl-Luciferins for Improved Bioluminescence Imaging. *Nat. Commun.* **2018**, *9*, 132.
(34) Yadav, A. K.; Lee, M. C.; Lucero, M. Y.; Su, S.; Reinhardt, C. J.; Chan, J. Activity-Based NIR Bioluminescence Probe Enables Discovery of Diet-Induced Modulation of the Tumor Microenvironment via Nitric Oxide. *ACS Cent. Sci.* **2022**, *8*, 461−472.
(35) Vieira, J.; Pinto da Silva, L.; Esteves da Silva, J. C. G. Advances in the Knowledge of Light Emission by Firefly Luciferin and Oxyluciferin. *J. Photochem. Photobiol. B Biol.* **2012**, *117*, 33−39.
(36) Kaskova, Z. M.; Tsarkova, A. S.; Yampolsky, I. V. 1001 Lights: Luciferins, Luciferases, Their Mechanisms of Action and Applications in Chemical Analysis, Biology and Medicine. *Chem. Soc. Rev.* **2016**, *45*, 6048−6077.
(37) Mofford, D. M.; Adams, S. T.; Reddy, G. S. K. K.; Reddy, G. R.; Miller, S. C. Luciferin Amides Enable *in Vivo* Bioluminescence Detection of Endogenous Fatty Acid Amide Hydrolase Activity. *J. Am. Chem. Soc.* **2015**, *137*, 8684−8687.
(38) Meisenheimer, P. L.; Uyeda, H. T.; Ma, D.; Sobol, M.; McDougall, M. G.; Corona, C.; Simpson, D.; Klaubert, D. H.; Cali, J. J. Proluciferin Acetals as Bioluminogenic Substrates for Cytochrome P450 Activity and Probes for CYP3A Inhibition. *Drug Metab. Dispos.* **2011**, *39*, 2403−2410.
(39) Wang, D.-D.; Jin, Q.; Zou, L.-W.; Hou, J.; Lv, X.; Lei, W.; Cheng, H.-L.; Ge, G.-B.; Yang, L. A Bioluminescent Sensor for Highly Selective and Sensitive Detection of Human Carboxylesterase 1 in Complex Biological Samples. *Chem. Commun.* **2016**, *52*, 3183−3186.
(40) Wang, D.-D.; Zou, L.-W.; Jin, Q.; Guan, X.-Q.; Yu, Y.; Zhu, Y.-D.; Huang, J.; Gao, P.; Wang, P.; Ge, G.-B.; Yang, L. Bioluminescent Sensor Reveals That Carboxylesterase 1A Is a Novel Endoplasmic Reticulum-Derived Serologic Indicator for Hepatocyte Injury. *ACS Sens.* **2020**, *5*, 1987−1995.
(41) Carl, P. L.; Chakravarty, P. K.; Katzenellenbogen, J. A. A Novel Connector Linkage Applicable in Prodrug Design. *J. Med. Chem.* **1981**, *24*, 479−480.
(42) Yan, J.; Lee, S.; Zhang, A.; Yoon, J. Self-Immolative Colorimetric, Fluorescent and Chemiluminescent Chemosensors. *Chem. Soc. Rev.* **2018**, *47*, 6900−6916.
(43) Lie Ken Jie, M. S. F.; Leung, D. W. Y. Preparation of 1-Phenyl Alkyl Esters of Medium and Long-Chain Fatty Acids. *Chem. Phys. Lipids* **1989**, *50*, 155−161.
(44) Tran, D. N.; Battilocchio, C.; Lou, S.-B.; Hawkins, J. M.; Ley, S. V. Flow Chemistry as a Discovery Tool to Access Sp^2 −Sp^3 Cross-Coupling Reactions via Diazo Compounds. *Chem. Sci.* **2015**, *6*, 1120−1125.

https://doi.org/10.1021/jacs.2c12984
J. Am. Chem. Soc. 2023, 145, 1460−1469

(45) Tsakos, M.; Schaffert, E. S.; Clement, L. L.; Villadsen, N. L.; Poulsen, T. B. Ester Coupling Reactions – an Enduring Challenge in the Chemical Synthesis of Bioactive Natural Products. *Nat. Prod. Rep.* **2015**, *32*, 605–632.
(46) Xiao, Q.; Zhou, Q.; Yang, L.; Tian, Z.; Wang, X.; Xiao, Y.; Shi, D. Breed Differences in Pig Liver Esterase (PLE) between Tongcheng (Chinese Local Breed) and Large White Pigs. *Sci. Rep.* **2018**, *8*, 16364.
(47) Martínez-Martínez, M.; Coscolín, C.; Santiago, G.; Chow, J.; Stogios, P. J.; Bargiela, R.; Gertler, C.; Navarro-Fernández, J.; Bollinger, A.; Thies, S.; Méndez-García, C.; Popovic, A.; Brown, G.; Chernikova, T. N.; García-Moyano, A.; Bjerga, G. E. K.; Pérez-García, P.; Hai, T.; Del Pozo, M. V.; Stokke, R.; Steen, I. H.; Cui, H.; Xu, X.; Nocek, B. P.; Alcaide, M.; Distaso, M.; Mesa, V.; Peláez, A. I.; Sánchez, J.; Buchholz, P. C. F.; Pleiss, J.; Fernández-Guerra, A.; Glöckner, F. O.; Golyshina, O. V.; Yakimov, M. M.; Savchenko, A.; Jaeger, K.-E.; Yakunin, A. F.; Streit, W. R.; Golyshin, P. N.; Guallar, V.; Ferrer, M.; The INMARE Consortium. Determinants and Prediction of Esterase Substrate Promiscuity Patterns. *ACS Chem. Biol.* **2018**, *13*, 225–234.
(48) Koźmiński, P.; Halik, P. K.; Chesori, R.; Gniazdowska, E. Overview of Dual-Acting Drug Methotrexate in Different Neurological Diseases, Autoimmune Pathologies and Cancers. *Int. J. Mol. Sci.* **2020**, *21*, 3483.
(49) El-Kalyoubi, S.; Agili, F. Synthesis, In Silico Prediction and In Vitro Evaluation of Antitumor Activities of Novel Pyrido[2,3-d]Pyrimidine, Xanthine and Lumazine Derivatives. *Molecules* **2020**, *25*, 5205.
(50) Cao, J.; Campbell, J.; Liu, L.; Mason, R. P.; Lippert, A. R. In Vivo Chemiluminescent Imaging Agents for Nitroreductase and Tissue Oxygenation. *Anal. Chem.* **2016**, *88*, 4995–5002.
(51) Qin, W.; Xu, C.; Zhao, Y.; Yu, C.; Shen, S.; Li, L.; Huang, W. Recent Progress in Small Molecule Fluorescent Probes for Nitroreductase. *Chin. Chem. Lett.* **2018**, *29*, 1451–1455.
(52) Gardner, S. H.; Brady, C. J.; Keeton, C.; Yadav, A. K.; Mallojjala, S. C.; Lucero, M. Y.; Su, S.; Yu, Z.; Hirschi, J. S.; Mirica, L. M.; Chan, J. A General Approach to Convert Hemicyanine Dyes into Highly Optimized Photoacoustic Scaffolds for Analyte Sensing**. *Angew. Chem., Int. Ed.* **2021**, *60*, 18860–18866.
(53) Fife, T. H.; Przystas, T. J. Divalent Metal Ion Catalysis in the Hydrolysis of Esters of Picolinic Acid. Metal Ion Promoted Hydroxide Ion and Water Catalyzed Reactions. *J. Am. Chem. Soc.* **1985**, *107*, 1041–1047.
(54) Denny, W. A. Nitroaromatic Hypoxia-Activated Prodrugs for Cancer Therapy. *Pharmaceuticals* **2022**, *15*, 187.
(55) Chen, S.; Xiao, L.; Li, Y.; Qiu, M.; Yuan, Y.; Zhou, R.; Li, C.; Zhang, L.; Jiang, Z.; Liu, M.; Zhou, X. In Vivo Nitroreductase Imaging via Fluorescence and Chemical Shift Dependent ^{19} F NMR. *Angew. Chem., Int. Ed. Engl.* **2022**, *61*, No. e202213495.
(56) Godet, I.; Doctorman, S.; Wu, F.; Gilkes, D. M. Detection of Hypoxia in Cancer Models: Significance, Challenges, and Advances. *Cell* **2022**, *11*, 686.
(57) Lopci, E.; Grassi, I.; Chiti, A.; Nanni, C.; Cicoria, G.; Toschi, L.; Fonti, C.; Lodi, F.; Mattioli, S.; Fanti, S. PET Radiopharmaceuticals for Imaging of Tumor Hypoxia: A Review of the Evidence. *Am. J. Nucl. Med. Mol. Imaging* **2014**, *4*, 365–384.
(58) Muz, B.; de la Puente, P.; Azab, F.; Azab, A. K. The Role of Hypoxia in Cancer Progression, Angiogenesis, Metastasis, and Resistance to Therapy. *Hypoxia (Auckl.)* **2015**, *3*, 83–92.
(59) Porterfield, W. B.; Jones, K. A.; McCutcheon, D. C.; Prescher, J. A. A "Caged" Luciferin for Imaging Cell–Cell Contacts. *J. Am. Chem. Soc.* **2015**, *137*, 8656–8659.
(60) Vorobyeva, A. G.; Stanton, M.; Godinat, A.; Lund, K. B.; Karateev, G. G.; Francis, K. P.; Allen, E.; Gelovani, J. G.; McCormack, E.; Tangney, M.; Dubikovskaya, E. A. Development of a Bioluminescent Nitroreductase Probe for Preclinical Imaging. *PLoS One* **2015**, *10*, No. e0131037.
(61) Wong, R. H. F.; Kwong, T.; Yau, K.-H.; Au-Yeung, H. Y. Real Time Detection of Live Microbes Using a Highly Sensitive Bioluminescent Nitroreductase Probe. *Chem. Commun.* **2015**, *51*, 4440–4442.
(62) Yang, K.; Leslie, K. G.; Kim, S. Y.; Kalionis, B.; Chrzanowski, W.; Jolliffe, K. A.; New, E. J. Tailoring the Properties of a Hypoxia-Responsive 1,8-Naphthalimide for Imaging Applications. *Org. Biomol. Chem.* **2018**, *16*, 619–624.
(63) Rathbun, C. M.; Prescher, J. A. Bioluminescent Probes for Imaging Biology beyond the Culture Dish. *Biochemistry* **2017**, *56*, 5178–5184.
(64) O'Sullivan, J. J.; Medici, V.; Heffern, M. C. A Caged Imidazopyrazinone for Selective Bioluminescence Detection of Labile Extracellular Copper(<scp>ii</Scp>). *Chem. Sci.* **2022**, *13*, 4352–4363.
(65) O'Sullivan, J. J.; Heffern, M. C. Development of an ATP-Independent Bioluminescent Probe for Detection of Extracellular Hydrogen Peroxide. *Org. Biomol. Chem.* **2022**, *20*, 6231–6238.
(66) Aron, A. T.; Heffern, M. C.; Lonergan, Z. R.; Vander Wal, M. N.; Blank, B. R.; Spangler, B.; Zhang, Y.; Park, H. M.; Stahl, A.; Renslo, A. R.; Skaar, E. P.; Chang, C. J. In Vivo Bioluminescence Imaging of Labile Iron Accumulation in a Murine Model of *Acinetobacter Baumannii* Infection. *Proc. Natl. Acad. Sci. U. S. A.* **2017**, *114*, 12669–12674.
(67) Monsees, T.; Miska, W.; Geiger, R. Synthesis and Characterization of a Bioluminogenic Substrate for α-Chymotrypsin. *Anal. Biochem.* **1994**, *221*, 329–334.
(68) Dragulescu-Andrasi, A.; Liang, G.; Rao, J. In Vivo Bioluminescence Imaging of Furin Activity in Breast Cancer Cells Using Bioluminogenic Substrates. *Bioconjugate Chem.* **2009**, *20*, 1660–1666.
(69) Kojima, R.; Takakura, H.; Kamiya, M.; Kobayashi, E.; Komatsu, T.; Ueno, T.; Terai, T.; Hanaoka, K.; Nagano, T.; Urano, Y. Development of a Sensitive Bioluminogenic Probe for Imaging Highly Reactive Oxygen Species in Living Rats. *Angew. Chem., Int. Ed.* **2015**, *54*, 14768–14771.
(70) Tian, X.; Li, Z.; Lau, C.; Lu, J. Visualization of in Vivo Hydrogen Sulfide Production by a Bioluminescence Probe in Cancer Cells and Nude Mice. *Anal. Chem.* **2015**, *87*, 11325–11331.
(71) Li, J.-B.; Chen, L.; Wang, Q.; Liu, H.-W.; Hu, X.-X.; Yuan, L.; Zhang, X.-B. A Bioluminescent Probe for Imaging Endogenous Peroxynitrite in Living Cells and Mice. *Anal. Chem.* **2018**, *90*, 4167–4173.
(72) Heffern, M. C.; Park, H. M.; Au-Yeung, H. Y.; Van de Bittner, G. C.; Ackerman, C. M.; Stahl, A.; Chang, C. J. In Vivo Bioluminescence Imaging Reveals Copper Deficiency in a Murine Model of Nonalcoholic Fatty Liver Disease. *Proc. Natl. Acad. Sci. U. S. A.* **2016**, *113*, 14219–14224.
(73) Van de Bittner, G. C.; Dubikovskaya, E. A.; Bertozzi, C. R.; Chang, C. J. In Vivo Imaging of Hydrogen Peroxide Production in a Murine Tumor Model with a Chemoselective Bioluminescent Reporter. *Proc. Natl. Acad. Sci. U. S. A.* **2010**, *107*, 21316–21321.
(74) Van de Bittner, G. C.; Bertozzi, C. R.; Chang, C. J. Strategy for Dual-Analyte Luciferin Imaging: *In Vivo* Bioluminescence Detection of Hydrogen Peroxide and Caspase Activity in a Murine Model of Acute Inflammation. *J. Am. Chem. Soc.* **2013**, *135*, 1783–1795.
(75) Cohen, A. S.; Dubikovskaya, E. A.; Rush, J. S.; Bertozzi, C. R. Real-Time Bioluminescence Imaging of Glycans on Live Cells. *J. Am. Chem. Soc.* **2010**, *132*, 8563–8565.
(76) Ticho, A. L.; Lee, H.; Gill, R. K.; Dudeja, P. K.; Saksena, S.; Lee, D.; Alrefai, W. A. A Novel Bioluminescence-Based Method to Investigate Uptake of Bile Acids in Living Cells. *Am. J. Physiol. Gastrointest. Liver Physiol.* **2018**, *315*, G529–G537.
(77) Henkin, A. H.; Cohen, A. S.; Dubikovskaya, E. A.; Park, H. M.; Nikitin, G. F.; Auzias, M. G.; Kazantzis, M.; Bertozzi, C. R.; Stahl, A. Real-Time Noninvasive Imaging of Fatty Acid Uptake *in Vivo*. *ACS Chem. Biol.* **2012**, *7*, 1884–1891.
(78) Wender, P. A.; Goun, E. A.; Jones, L. R.; Pillow, T. H.; Rothbard, J. B.; Shinde, R.; Contag, C. H. Real-Time Analysis of Uptake and Bioactivatable Cleavage of Luciferin-Transporter Conjugates in Transgenic Reporter Mice. *Proc. Natl. Acad. Sci. U. S. A.* **2007**, *104*, 10340–10345.

(79) Sellmyer, M. A.; Bronsart, L.; Imoto, H.; Contag, C. H.; Wandless, T. J.; Prescher, J. A. Visualizing Cellular Interactions with a Generalized Proximity Reporter. *Proc. Natl. Acad. Sci. U. S. A.* **2013**, *110*, 8567−8572.
(80) Yao, H.; So, M.; Rao, J. A Bioluminogenic Substrate for In Vivo Imaging of β-Lactamase Activity. *Angew. Chem., Int. Ed.* **2007**, *46*, 7031−7034.
(81) Zhou, W.; Shultz, J. W.; Murphy, N.; Hawkins, E. M.; Bernad, L.; Good, T.; Moothart, L.; Frackman, S.; Klaubert, D. H.; Bulleit, R. F.; Wood, K. V. Electrophilic Aromatic Substituted Luciferins as Bioluminescent Probes for Glutathione S-Transferase Assays. *Chem. Commun.* **2006**, *44*, 4620−4622.
(82) Li, J.; Chen, L.; Du, L.; Li, M. Cage the Firefly Luciferin! − A Strategy for Developing Bioluminescent Probes. *Chem. Soc. Rev.* **2013**, *42*, 662−676.
(83) Miska, W.; Geiger, R. Synthesis and Characterization of Luciferin Derivatives for Use in Bioluminescence Enhanced Enzyme Immunoassays. New Ultrasensitive Detection Systems for Enzyme Immunoassays, I. *J. Clin. Chem. Clin. Biochem.* **1987**, *25*, 23−30.
(84) Geiger, R.; Schneider, E.; Wallenfels, K.; Miska, W. A New Ultrasensitive Bioluminogenic Enzyme Substrate for β -Galactosidase. *Biol. Chem. Hoppe-Seyler* **1992**, *373*, 1187−1192.
(85) Endo, M.; Ozawa, T. Advanced Bioluminescence System for In Vivo Imaging with Brighter and Red-Shifted Light Emission. *Int. J. Mol. Sci.* **2020**, *21*, 6538.

https://doi.org/10.1021/jacs.2c12984
J. Am. Chem. Soc. 2023, 145, 1460−1469